Giant dipole resonances built on superdeformed rotational states

Y. S. Chen
Institute of Atomic Energy, Beijing, China
(Received 2 January 1990)

The structure and properties of the superdeformed giant dipole resonances (SDGDR) in rotating $^{146-152}$Dy, $^{132-136}$Nd, and $^{80-84}$Sr even nuclei are studied based on the linear-response theory with self-consistently determined superdeformed mean field. The effect of γ deformation as well as the triaxial superdeformation on the SDGDR is also investigated. The obtained common features may serve as the criterion for the observation of the SDGDR. The features are understood at a microscopic level by analyzing the distributions of the unperturbed p-h pairs connected with $E1$ operators.

I. INTRODUCTION

The giant dipole resonances (GDR) in the γ-ray spectra following heavy-ion fusion reaction (HI,xn) provides an exciting opportunity to study the properties of hot rotating nuclei, particularly nuclear shapes varying with increasing temperature and spin as well as thermal shape fluctuation. The first measurement of GDR structured on nuclear high spin states was made at LBL.[1] The first clear evidence that deformation plays an important role in determining the GDR shape in highly rotating nuclei came from the Neils Bohr Institute (NBI) experiment[2] on the decay of the compound nucleus ^{108}Sn*. A recent series of experiments at Seattle[3] apply the systematic of the GDR at $T=1-2$ MeV and $I=(0-25)\hbar$, in a wide variety of excited nuclei from $A=46$ to 166. All these are for normally deformed nuclei. The first superdeformed (SD) rotational band was found in ^{152}Dy at Daresbury;[4] the ratio between the long and short axes of nucleus is about 2:1. Since then more and more superdeformed nuclei were discovered at high spins in $A=130$, 150, and 190 regions; for example, see Ref. 5 and references therein. It is very interesting to search for the GDR built on the SD states (SDGDR). It is not only the subject of discovering a new kind of the GDR but also the subject related with the question of whether the SD states are populated by means of the decay of the SDGDR in the heavy-ion fusion reactions. A very recent experiment[6] on the decay of the GDR in ^{156}Dy* reported no convincing evidence for the SDGDR in the residual nucleus ^{152}Dy which was found to be superdeformed in the yrast spectroscopy study. This indicates the very difficulties of such observations, for the SD intensity is very weak, generally less than 1% of the total γ-ray intensity in the rare-earth nuclei. Thus more quantitative and detailed theoretical studies are necessary and helpful for such observations of the SDGDR in a sense. The GDR in normally deformed hot rotating nuclei has been studied theoretically in detail; however, only very limited work has been carried out concerning the GDR built on superdeformed states. This article presents the theoretical results of the SDGDR in $^{146-152}$Dy, $^{132-136}$Nd, and $^{80-84}$Sr even nuclei, calculated by the linear-response theory based on the cranking mean field. The model is described briefly in Sec. II. The results and discussions are given in Sec. III. The summary is in Sec. IV.

II. THE MODEL

The present SDGDR calculations are based on the thermal linear-response theory, which is equivalent to thermal RPA and has been tentatively used as a powerful technique to study the GDR in hot rotating nuclei; for example, see Refs. 7–10. The calculations include the following procedure: (1) to calculate nuclear shapes at each angular momentum self-consistently with respect to ε_2 and γ deformations by the cranking-shell-model calculation of Sturtinsky type;[11] (2) to calculate the intrinsic photon absorption cross sections for the $E1$ dipole excitation modes associated with the equilibrium superdeformed field which is obtained in step (1), by solving the equation of deformed dipole response function at a finite temperature and without pairing; (3) to make transformations for the cross sections from the intrinsic into the laboratory frame.

The shape of the GDR is mainly determined by the deformation of nuclear states on which the GDR is structured. The temperature and rotational motion have only a small effect on both the centroid energy and the width of the GDR for a fixed deformation, but they may indirectly have a strong effect, namely, through inducing the deformation changes and thermal shape fluctuation. Therefore, it is necessary to calculate nuclear shapes self-consistently in a completed GDR study. The validity of neglecting pairing in the random-phase-approximation (RPA) calculation is found from the fact that the yrast SD states are formed at very high spins, where the pairing, at least the static pairing, is collapsed or strongly weakened. And besides, the pairing plays a negligible role in determining the shape of the GDR once the deformation is fixed. In fact, to include the pairing in the calculation of nuclear shape is more meaningful than in the RPA calculation. The thermal effect is also not considered in the self-consistent calculations of nuclear shapes, because the SD minimum is found to be not sensitive to a finite temperature T. We have checked and found by the thermal cranking model calculation of the total free energy surface that the SD minimum at very

high spins is flat and cannot persist at higher temperature, and is basically washed out at $T>0.5$ MeV in considered nuclei. Thus it is expected that the SDGDR may be only observable in a cold nucleus. Therefore, it may be more instructive to present the calculated results of zero temperature, while the effect of a finite temperature on the SDGDR is discussed in spite of the doubt about the existence of SDGDR at higher temperature. The results presented in the present article are for zero temperature, otherwise it must be stated. The thermal effect is included in the calculations of photon absorption cross sections by taking into account the thermal occupation numbers $n_\alpha(T)$, and the thermal shape fluctuation which makes the width of the GDR broadening[9] is not considered in the present study.

With the above physical considerations, the Hamiltonian of a deformed system with a dipole-dipole separable effective interaction may be written as

$$H=h(d)-\omega_{\rm rot} j_1+\sum_\mu \chi_\mu D_\mu^+ D_\mu \ , \tag{1}$$

where the first two terms describe the single-particle motion in a superdeformed potential rotating around an intrinsic axis 1 with a rotational frequency $\omega_{\rm rot}$, and j_1 is the projection of single-particle angular momentum along the axis 1. The deformation parameters ε_2, ε_4, and γ are abbreviated to "d". The third term in (1) is the dipole-dipole residual interaction. The coupling strength parameters χ_μ, $\mu=1,2,3$, differ from each other along different axis μ for a deformed nucleus.

We assume that the deformed rotating mean field in (1) is of reflection symmetry. Thus only the dipole-dipole interaction term in (1) contributes to the thermal RPA equation since the GDR is formed by the excitation of negative parity. This allows us to determine the superdeformed mean field, namely, the deformation parameters d, in advance by an appropriate way, and afterwards to solve the RPA equation just as an individual problem. By solving the eigenequation of the first two terms in (1) one obtains the single-particle energies e_α^ω and the corresponding wave functions $|\alpha\rangle$. According to the cranking model, the total angular momentum of the nucleus may be calculated as the expectation value of j_1 operator $I=I_1=\sum\langle\alpha|j_1|\alpha\rangle$, where the summation runs over all levels occupied by nucleons. The resulting single-particle states are employed as the basis in which the thermal RPA equation of Hamiltonian (1) is solved in the framework of linear-response theory.

The response function $R(E)$, describing the response of the system to an external dipole radiation field with energy E, is given by the linear-response equation[12]

$$R=R^0+R^0\chi R \ , \tag{2}$$

where χ is a diagonal matrix whose elements are $\chi_{\mu\nu}=\chi_\mu\delta_{\mu\nu}$. R^0 is the response matrix without residual interaction ($\chi_\mu=0$), whose elements are given by

$$R^0_{\mu\nu}(E)=\sum_{\alpha,\beta}\frac{\langle a|D_\mu|\beta\rangle^*\langle a|D_\nu|\beta\rangle[n_\beta(T)-n_\alpha(T)]}{E-e_\alpha^\omega+e_\beta^\omega+i\Gamma/2} \ , \tag{3}$$

where the thermal occupation factor $n_\alpha(T)=1/\{1+\exp[e_\alpha^\omega-\lambda/T]\}$ gives the probability for thermally exciting a particle. In general, Γ in (3) is an operator describing the very complicated couplings which are impossible to treat exactly in practice. Here we introduce a phenomenological width representing the coupling to more complicated configurations, the decay width, and the continuum, the escape width. $\Gamma=1$ MeV is taken in the present calculations as a reasonable value.

The reflection symmetry of a deformed system leads to the response matrix $R(E)$ reducing into a 1×1 determinant containing the R_{11} and a 2×2 determinant containing the rest. The matrix equation (2) can be easily solved by inverting the matrix. We chose the laboratory frame such that the laboratory frame is oriented by the Euler angles $(0,\pi/2,\pi/2)$ with respect to the intrinsic frame. The spherical tensor dipole operators in the laboratory frame are

$$\begin{bmatrix} D_+ \\ D_0 \\ D_- \end{bmatrix}=\begin{bmatrix} 0 & -1/\sqrt{2} & -i1/\sqrt{2} \\ 1 & 0 & 0 \\ 0 & 1/\sqrt{2} & -i1/\sqrt{2} \end{bmatrix}\begin{bmatrix} D_1 \\ D_2 \\ D_3 \end{bmatrix} . \tag{4}$$

Here the phase convention has been chosen so that under the time-reverse transformation $TD_\mu T^{-1}=-D_\mu$, $\mu=1,2,3$. D_+, D_0, and D_- give rise to the $E1$ transitions of I to $I+1$, I, and $I-1$, respectively, in the laboratory frame. Transforming the dipole operators, as (4), and the $E1$ transition energy from the intrinsic to the laboratory frame one finds the following expression for the photon absorption cross section in the laboratory frame:

$$\sigma(E)=\sigma_{D_0}(E)+\sigma_{D_+}(E-\hbar\omega_{\rm rot})+\sigma_{D_-}(E+\hbar\omega_{\rm rot}) \ , \tag{5}$$

$$\sigma_{D_s}(E)=-4\pi(e^2/\hbar c)E\ {\rm Im}[R_{D_sD_s}(E)] \ . \tag{6}$$

The response matrix element $R_{D_sD_s}$ may be calculated from the elements of R by

$$\begin{bmatrix} R_{D_+D_+} \\ R_{D_0D_0} \\ R_{D_-D_-} \end{bmatrix}=\begin{bmatrix} \frac{1}{2} & 0 & i\frac{1}{2} \\ 0 & 1 & 0 \\ \frac{1}{2} & 0 & -i\frac{1}{2} \end{bmatrix}\begin{bmatrix} R_{22}+R_{33} \\ R_{11} \\ R_{23}-R_{32} \end{bmatrix} . \tag{7}$$

III. THE RESULTS OF CALCULATIONS

The Modified Harmonic Oscillator (MHO) potential is used in the RPA calculation. The Nilsson potential parameters κ and μ employed in the present calculations are listed in Table I. We have checked that the GDR results are not sensitive to κ and μ in the range of reasonable values. The coupling strength χ_μ can be calculated as (Ref. 13) $\chi_\mu=x(3A/NZ)M\omega_0^2(\mu)$, $\mu=1,2,3$, where $\omega_0(\mu)$ is the oscillator frequency which is inversely proportional to the extension of the nucleus along the axis μ. The assumption of the volume conservation requires $\hbar[\omega_0(1)\omega_0(2)\omega_0(3)]^{1/3}=41A^{-1/3}$ MeV. For a deformed heavy nucleus, the dimensionless quantity $x<1$, usually x is adjusted to the main peak of the experimentally observed GDR based on the ground state. Since such data

TABLE I. The Nilsson potential parameters used in the calculations of the GDR and the shapes of Dy nuclei.

	Protons		Neutrons	
N	κ	μ	κ	μ
0	0.120	0.00	0.120	0.00
1	0.120	0.00	0.120	0.00
2	0.105	0.00	0.105	0.00
3	0.085	0.34	0.095	0.28
4	0.064	0.60	0.070	0.40
5	0.060	0.58	0.067	0.42
6	0.058	0.56	0.065	0.42
7	0.056	0.54	0.062	0.38
8	0.054	0.54	0.062	0.34

are not available in considered nuclei, we chose an empirical value $x=0.75$, 0.65, and 0.5 for Dy, Nd, and Sr nuclei, respectively. With these values of parameter x, the present model calculation yields a reasonable mass A dependence of the resonance energies, which coincides with the systematic of the GDR energies for normally deformed nuclei, as given in Ref. 3. The single-particle space for the GDR calculation includes nearly three major shells of (proton $N=3-7$ and neutron $N=4-8$) in Dy nuclei, of (proton $N=2-6$ and neutron $N=3-7$) in Nd nuclei, and of (proton $N=2-6$ and neutron $N=2-6$) in Sr nuclei, respectively.

The present shape calculations are carried out with Nilsson potential and without pairing ($\Delta=0$) for Dy nuclei, while with a more realistic Woods-Saxon potential and with a phenomenological rotational frequency ω-dependent pairing for both Nd and Sr nuclei. We take $\Delta(\omega)=\Delta_0[1-0.5(\omega/\omega_c)^2]$ for $\omega<\omega_c$ and $\Delta(\omega)=0.5\Delta_0(\omega/\omega_c)^2$ for $\omega>\omega_c$. ω_c is taken to be 0.7 MeV for both Nd and Sr nuclei in the calculation; for the details refer to Ref. 14 and references therein. Both methods are good enough in determining SD nuclear shapes at very high spins for the purpose of the study. The hexadecapole deformation ε_4 is fixed and the self-consistent calculation is carried out with respect to ε_2 and γ deformations.

A. Superdeformation

The deformation parameter ε_4 is set to zero for the calculations of the SD shapes of Dy nuclei and is taken as the liquid-drop value in the calculations of SD shapes of both Nd and Sr nuclei for simplicity. The shape calculations result in nearly prolate superdeformed shapes for the yrast states in $^{146-152}$Dy even nuclei at the angular momenta from $60\hbar$ to $70\hbar$, and for the yrast states in $^{132-136}$Nd even nuclei at the angular momentum around $32\hbar$ and the yrast states in $^{80-82}$Sr nuclei at the angular momenta round $44\hbar$. However, the yrast state of ^{84}Sr is found to have a superdeformed triaxial shape at the angular momentum $I=48\hbar$. The corresponding values of ε_2 and γ together with the angular momenta $I_{\min}$ where the SD states become yrast are listed in Table II.

TABLE II. The calculated superdeformation parameters and the angular momentum $I_{\min}$ where the SD state becomes yrast.

Nucleus	ε_2	γ	ε_4	$I_{\min}$ ($\hbar$)
^{146}Dy	0.45	6°	0.00	62
^{148}Dy	0.48	4°	0.00	64
^{150}Dy	0.55	5°	0.00	68
^{152}Dy	0.56	3°	0.00	64
^{132}Nd	0.32	3°	0.011	32
^{134}Nd	0.34	3°	0.020	32
^{136}Nd	0.32	3°	0.025	34
^{80}Sr	0.43	7°	0.014	44
^{82}Sr	0.47	5°	0.017	44
^{84}Sr	0.41	48°	0.009	48

B. Photon absorption cross section

In the phenomenological two fluid hydrodynamic model,[15] the GDR is a collective oscillation of proton and neutron fluids within the fixed boundaries of a rigid deformed shape. The peak energies are inversely proportional to the extension of the nucleus along each axis. For the superdeformed prolate shape, one expects two components of the GDR far apart in energy. This feature is revealed in the calculated total photon absorption cross sections presented in Fig. 1. The relative frac-

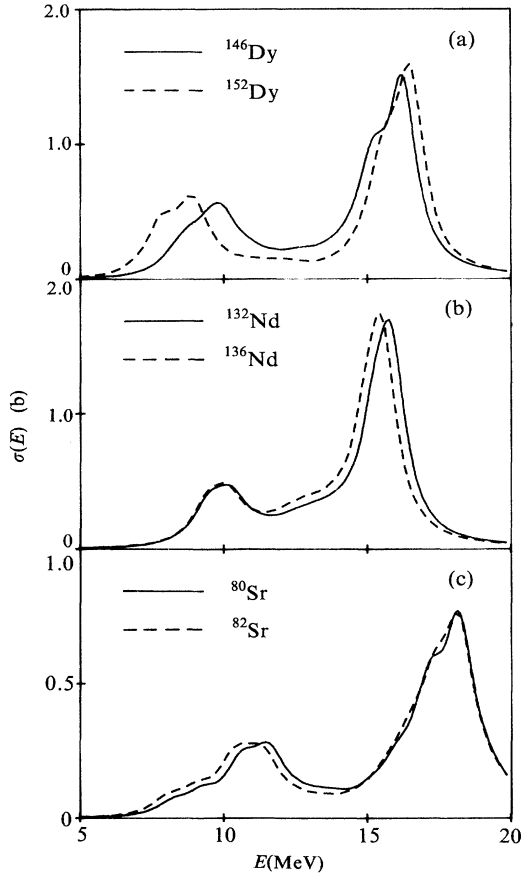

FIG. 1. Total photon absorption cross section in the laboratory frame associated with the SDGDR: (a) for ^{146}Dy at $I=62\hbar$ (solid) and ^{152}Dy at $I=64\hbar$ (dashed); (b) for ^{132}Nd at $I=32\hbar$ (solid) and ^{136}Nd at $I=34\hbar$ (dashed); (c) for ^{80}Sr (solid) and ^{82}Sr (dashed) at $I=44\hbar$.

tion of the energy-weighted sum rule (EWSR) presented in the low-energy component is about 32% in $^{146-152}$Dy, being the value characteristic of a prolate shape. The full width at half maximum (FWHM) of the absorption cross section is about 2.5 MeV for the low-energy component and 2 MeV for the high-energy component. It is seen from Fig. 1(a) that the splitting is about 1.5 MeV larger for ^{152}Dy than for ^{146}Dy. Obviously, this is because of the deformation ε_2 in ^{152}Dy being larger than that in ^{146}Dy. The SDGDR in ^{152}Dy was previously studied in Ref. 9, and the present result, Fig. 1(a), is actually very similar to Fig. 8(D) of Ref. 9. The shape of the calculated total photon absorption cross section for ^{148}Dy (and ^{150}Dy) is almost the same as that for ^{146}Dy (and ^{152}Dy), respectively, and thus not plotted in Fig. 1(a) for a better view. This can be easily understood from the fact that the calculated deformations of ^{148}Dy (and ^{150}Dy) are very close to those of ^{146}D (and ^{152}Dy), respectively, as seen in Table II. The superdeformations for either $^{132-136}$Nd or $^{80-82}$Sr are close to each other; therefore, the SDGDR in either $^{132-136}$Nd or $^{80-82}$Sr have almost the same shape, as seen in Figs. 1(b) and 1(c). The relative fraction of the EWSR presented in the low-energy component is about 26% and 31% for Nd and Sr nuclei, respectively. The calculated FWHM of the low-energy peak is always larger than that of the high-energy peak in a SDGDR. The difference in the FWHM between the low- and high-energy components originates mainly from the difference of their fragmentation widths caused by rotational motion.

Figure 2 shows the total photon absorption cross sections for the SDGDR in ^{150}Dy, ^{134}Nd, and ^{82}Sr, plotted together with the decomposed three resonance shapes for the transition modes I to I and $I\pm1$. One observes in Fig. 2 that the low-energy component of the SDGDR almost only consists of transition modes I to $I\pm1$ since it is far apart in energy from the resonance of mode I to I, which contributes only to the high-energy component. Consequently, the low-energy component presents basically pure stretched $E1$ transitions, while the high-energy component is a mixture of all three modes and formed with a large fraction of nonstretched transitions.

The calculation shows that the temperature effects a little change in the shape of SDGDR for a fixed nuclear shape. The high-energy peak shifts down in energy about 0.5 MeV, but has almost no change in its strength and width when temperature increases from 0 to 1.0 MeV in ^{150}Dy. The low-energy component of SDGDR presents even a high persistency at higher temperature: The centroid energy, the strength, and width have only a negligible change when temperature increases up to 1.5 MeV.

C. Anisotropy of the angular distribution

The present model is based on the assumption that the hot rotating nucleus following the (HI,xn) reaction can be described statistically by introducing the picture of a finite temperature. The angular distribution of γ rays emitted from such a statistic system presents isotropic as a result of averaging over the final-state spin. For $E1$ dipole transitions in a system with $I \gg M$ and $I \gg 1$, here M is the projection of I along the beam axis, the angular distribution of the emitted γ rays relative to the beam axis is $W(\theta) \propto 1+a_2P_2(\cos(\theta))$ with $a_2=-0.25$ for $\Delta I=\pm1$ modes and 0.5 for the $\Delta I=0$ mode approximately. Thus the a_2 may be calculated as $a_2=0.75(\sigma_{D_0}/\sigma)-0.25$.

The anisotropy of angular distribution could occur for given I and E due to the deformation. The dipole vibration along the axis 1, the rotational axis, does not change angular momentum in the cranking limit $I=I_1$ and thus corresponds to the $\Delta I=0$ transition, while vibrations along the other two principal axes correspond to the $\Delta I=\pm1$ transitions in each case. Therefore, the energy splitting caused by the deformation will displace the $\Delta I=0$ and the $\Delta I=\pm1$ transition energies and leads to the anisotropy. For a similar reason, rotation itself also leads to an anisotropy, but the effect is very small. However, we should keep in mind that a rotation as well as a finite temperature may give rise to the change of the anisotropy through a large deformation change when rotation and temperature are provided for a nucleus. The

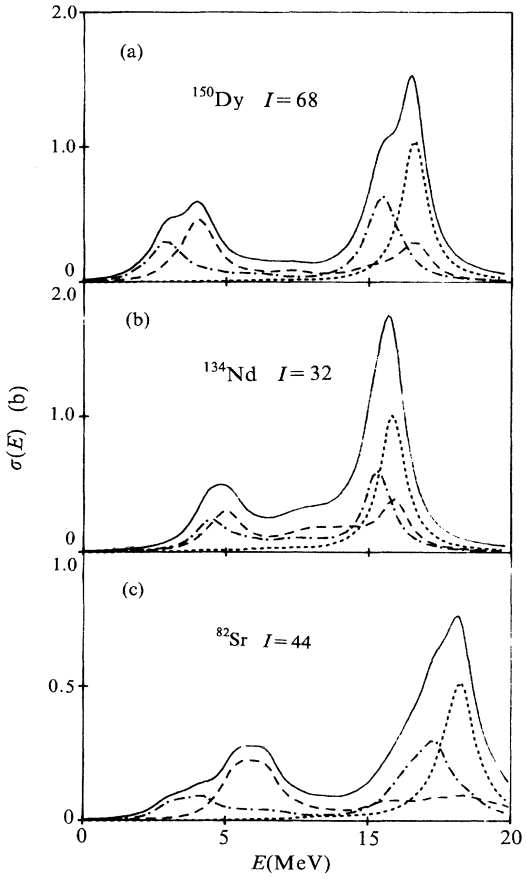

FIG. 2. Total photon absorption cross section in the laboratory frame associated with the SDGDR: (a) For ^{150}Dy at $I=68\hbar$; (b) For ^{134}Nd at $I=32\hbar$; (c) for ^{82}Sr at $44\hbar$. The decomposed three resonance shapes for transition modes I to I (dotted), I to $I+1$ (dashed), and I to $I-1$ (dot-dashed) are presented.

calculated anisotropy $W(90°)/W(145°)$ for the superdeformed nucleus ^{150}Dy at $I=68\hbar$ is shown in Fig. 3(a). The large anisotropy around 9 MeV, the value closing to the limit of pure stretched transitions, indicates that the low-energy component of the SDGDR is basically formed from the $E1$ decay of $\Delta I=\pm 1$ modes. This conclusion will hold even if more realistic resonance width is considered in the calculation. This may serve as a signal of the observation of the SDGDR in an experiment of a new type like that reported in Ref. 6. The large anisotropy (<1) is also found around 16.5 MeV where the high-energy component of the GDR gets the maximum. It reaches at a half of the nonstretched limit of anisotropy, about 0.6, as see in Fig. 3. Generally, the feature at high energy holds for the case of the normally deformed system. However, it is expected that the isotropic point, as an intersection point of the anisotropy curve and the isotropic line $W(90°)/W(145°)=1$, is displaced at higher energy for the superdeformation case than for the normal deformation case in the same nucleus as the resonance of $\Delta I=0$ is displaced much higher in energy for the former case. It is noted that the isotropic point may be shifted downward when the complex doorway coupling is included in the response function. But it is likely that the substantial upward shift of the isotropic point for the SDGDR may be a sign of superdeformation, because the isotropic point in the normal deformed GDR is hard to shift up to such a high energy due to the coupling to more complex configurations.

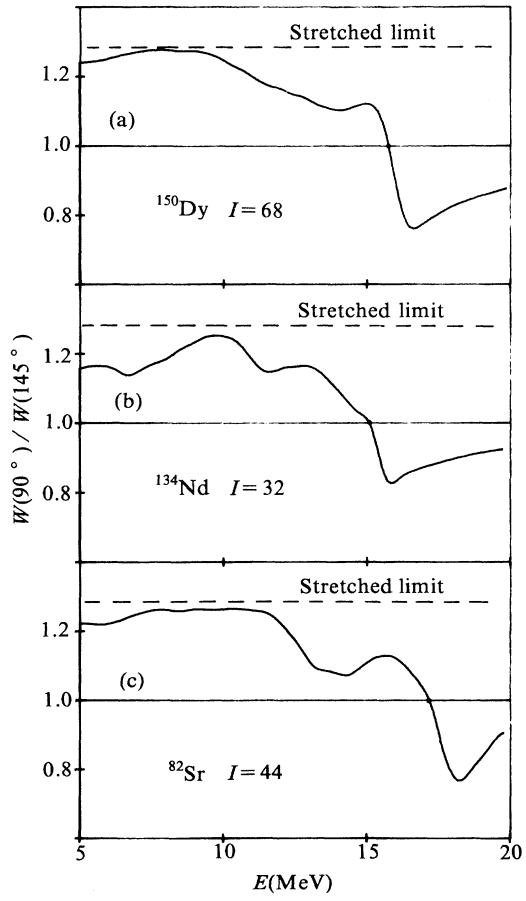

FIG. 3. The calculated anisotropy $W(90°)/W(145°)$ in the angular distribution of γ rays from the decay of the SDGDR: (a) for ^{150}Dy at $I=68\hbar$; (b) for ^{134}Nd at $I=32\hbar$; (c) for ^{82}Sr at $I=44\hbar$.

The calculated anisotropies $W(90°)/W(145°)$ for ^{134}Nd at $I=32\hbar$ and ^{82}Sr at $I=44\hbar$ are shown in Figs. 3(b) and 3(c), respectively. The overall structure of the anisotropy for either ^{134}Nd or ^{82}Sr is similar to that for ^{150}Dy. However, the large anisotropy around low-peak energies maintains up to higher energy as going from ^{150}Dy, ^{134}Nd, to ^{82}Sr, coinciding with their peak energies.

D. The p-h pair distribution

The large ε_2 deformation in SD states leads to very strong j mixture in the single-particle wave functions and consequently the $\Delta N=1$ p-h pair spherical configurations in higher N shell may contribute to the GDR more significantly in contrast to the normal deformation case. The exotic deformation together with rotation and temperature will lead to the tremendous number of the p-h pairs which have nonvanishing matrix elements of the $E1$ dipole operators. The patterns of the p-h pair distributions for $|\langle D_1\rangle|$, $|\langle D_2\rangle|$, and $|\langle D_3\rangle|$ each larger than zero are very similar to each other. However, this does not mean that the intrinsic photon absorption cross sections, which describe the vibrations along the principal axes 1, 2, and 3, respectively, will have similar structures. We must bear in mind that we are working in a limited p-h space and we should only look at the important p-h pairs which have the matrix elements of the $E1$ operators large enough so that they contribute to the GDR significantly. One can see from Fig. 4 that the most important p-h pairs which have large D_3 matrix elements are distributed as a narrow peak around the p-h excitation energy of about 5 MeV, as shown by the $|\langle D_3\rangle|>0.4$ curve in Fig. 4(c). These p-h configurations applied the unperturbed main microscopic structural bases of the lower-energy component of the SDGDR in ^{150}Dy. The important p-h pairs which have large D_1 and D_2 matrix elements are distributed as broad peaks around the p-h excitation energy of ~ 9 MeV as shown by the $|\langle D_1\rangle|>0.4$ and the $|\langle D_2\rangle|>0.4$ curves in Figs. 4(a) and 4(b), respectively. They provide the unperturbed main microscopic structural bases for the high-energy component of the SDGDR in ^{150}Dy.

From the calculations for ^{134}Nd and ^{82}Sr one finds that the most important p-h pairs which have large D_3 matrix elements are distributed as a narrow peak around the p-h excitation energy of about 6 MeV. The important p-h pairs which have large D_1 and D_2 matrix elements are distributed as broad peaks around the p-h excitation energies of ~ 8 (^{134}Nd) and ~ 11 (^{82}Sr) MeV.

Microscopically these important p-h pairs are presented with large amplitudes in the collective p-h doorway resonance which is a coherent superposition of p-h pair configurations. Including the repulsive interaction between particles and holes shifts the resonance energy up

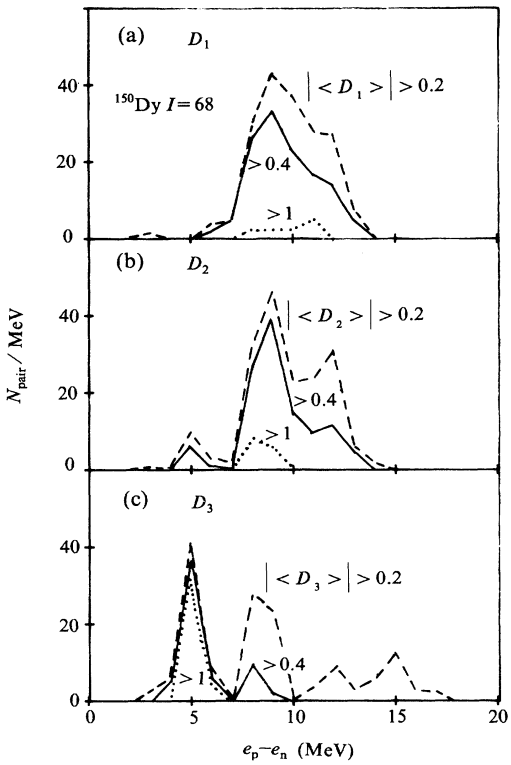

FIG. 4. The number of the p-h pairs, per MeV, which have large matrix elements of (a) D_1, (b) D_2, and (c) D_3, plotted versus the p-h excitation energy for $|\langle D_\mu \rangle| > 0.2$ (dashed), >0.4 (solid), and >1.0 (dotted) in the superdeformed ^{150}Dy at $I=68\hbar$.

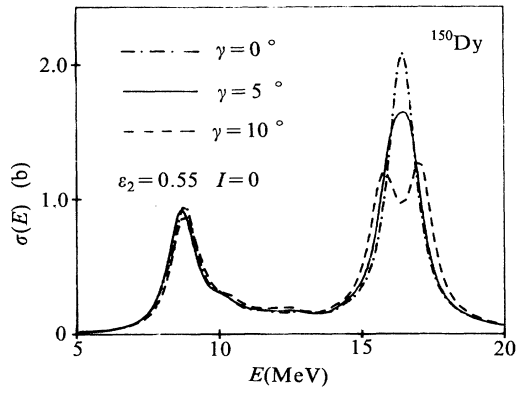

FIG. 5. Total photon cross sections calculated with the deformation parameters $\varepsilon_2=0.55$ and $\gamma=0°$ (dot-dashed), $\gamma=5°$ (solid), and $\gamma=10°$ (dashed) for ^{150}DY at $I=0$.

to observed values by a factor ~ 1.8. The large splitting of two peaks in the SDGDR may be estimated by the splitting of two peaks in the important p-h pair distribution with an enlargement factor of ~ 1.8.

E. Effect of γ deformation

The break of the axial symmetry, namely, the γ deformation, brings the K mixture into the wave functions of single-particle states and therefore leads to numbers of p-h pairs which have nonzero matrix elements of the $E1$ dipole operators and thus occasionally changes the distributions of the p-h pairs. The present calculation shows that even a small γ deformation will have a considerable effect on the high-energy component, but not on the low-energy component of the SDGDR. Figure 5 presents the total photon absorption cross sections for ^{150}Dy at I=0, calculated with three sets of deformation parameters, namely, same $\varepsilon_2=0.55$, but different γ values of 0°, 5°, and 10°. One finds that the low-energy component remains almost unchanged in both the peak strength, defined as the height of the resonance peak, and width, while considerable changes are observed in the peak strength and width of the high-energy component. The full width at half maximum of the high-energy component for $\gamma=0°$, 5°, and 10° is 1.1, 1.5, and 2.3 MeV, respectively. In contrast, the calculated increment of the FWHM of the high-energy component as a result of increasing I from 0 to $60\hbar$ is about 0.4 MeV. The increment of the fragmentation width which is caused by increasing the γ deformation just accounts for the increment of the calculated width since thermal shape fluctuation effect on the width is not included and the fragmentation of the GDR strength is treated microscopically in the model. The calculated width of the low-energy component is 1.4 MeV for all the three sets of deformation parameters. With increasing γ deformation, the peak strength of the high-energy component decreases while the peak strength of the low-energy component remains almost unchanged. Consequently, the calculated high-energy to low-energy peak strength ratio is 2.2:1 and 1.2:1 for $\gamma=0°$ and 10°, respectively. It should be noticed that the integrated strength, namely, the energy-weighted sum rule, does not vary much as γ deformation increases from 0° to 10°; the calculated high-energy to low-energy EWSR ratio is ~ 1.9 for $\gamma=10°$, still being the characteristic of the prolate shape. The effect remains when the rotation is included; the calculated FWHM of the high-energy component for $\gamma=0°$ and $\gamma=10°$ is 1.6 and 2.7 MeV, respectively, in ^{150}Dy at $I=64\hbar$. The peak splitting of two resonances in the high-energy component for $\gamma=10°$ as shown in Fig. 5 is even enhanced, but their peak strength differs more from each other due to the fast rotation. It should be noticed that the effect of such a small γ deformation may be washed out by including the more complex doorway couplings which are mostly associated with the broadening of the resonance. Nevertheless, the above results indicate that a small γ deformation leads to a considerable change in the shape of the resonance and thus a self-consistent calculation with respect to γ deformation is necessary in a detailed theoretical study of the SDGDR although the SD shape is expected to be near prolate at the considered region of angular momenta. The effect of the γ deformation can be understood microscopically by examining the distribution of important p-h pairs in their excitation energies similar to those presented in Fig. 4. For an axial symmetry case, the distribution of the p-h pairs connected by D_1 is the

same as that of the p-h pairs connected by D_2. However, a small γ deformation breaks the axial symmetry so that the distributions of important p-h pairs for D_1 and D_2 are no longer the same as each other. The calculation indicates that the p-h pairs connected by D_2 are distributed around lower excitation energies than for the p-h pairs connected by D_1. After the perturbation, this leads to the strength fragmentation in the high-energy component of SDGDR. In contrast, the distribution of the p-h pairs connected by D_3 presents almost no change and thus the low-energy component remains almost unchanged when the γ deformation varies from 0° to 10°.

The effect of the γ deformation on the high-energy component of the SDGDR may be also understood by simply examining the fragmentation of the oscillations along the axes 1 and 2. The difference of the oscillator frequencies is proportional to ε_2 deformation, $\Delta\hbar\omega_0 = \hbar\omega_0(1) - \hbar\omega_0(2) = 2/\sqrt{3}\varepsilon_2 \sin(\gamma)(41 A^{-1/3}$ MeV). For a small γ deformation the $\Delta\hbar\omega_0$, and therefore its resulting strength fragmentation, is small for the $\sin(\gamma)$ factor and its small ε_2 in the normal GDR, but becomes much more effective in the SDGDR for its very large ε_2 and the fact that the coupling strength is proportional to the square of $\omega_0(\mu)$.

It is expected for a superdeformed triaxial shape that the SDGDR has a completely different structure from that for a nearly prolate superdeformed shape. As an example, the present shape calculation results in a superdeformed triaxial shape for the yrast state of ^{84}Sr at $I = 48\hbar$, as listed in Table II. The calculated photon absorption cross section for ^{84}Sr at $I = 48\hbar$ is shown in Fig. 6(a). The decomposed three components for the transition modes $\Delta I = 0, \pm 1$ are plotted together in the same figure. As the characteristic of the superdeformation, again the SDGDR in ^{84}Sr has a large energy splitting between the low- and high-energy components. However, by comparing Figs. 2(c) and 6(a), one finds that the SDGDR in ^{84}Sr is so different from the SDGDR in ^{82}Sr in both their resonance energies and the widths. Moreover, considerable strength of the SDGDR in ^{84}Sr is distributed to bridge the valley between the low- and high-energy peaks, as demonstrated in Fig. 6(a). This is the characteristic of superdeformed triaxial shape. In fact, the extensions of a superdeformed triaxial nucleus along the three principle axes are so different that the corresponding dipole vibrations along the axes have well separated frequencies, and consequently the SDGDR has three components. The bridge is actually formed mainly from the γ rays emitted from deexcitation of the $E1$ vibrational motion along the axis 2. Both the low-energy component and the bridge are formed from $\Delta I = \pm 1$ transition γ rays, while the high-energy component is structured by very pure $\Delta I = 0$ transition γ rays. It is expected that the anisotropy of angular distribution $W(90°)/W(145°)$ reaches to the limit of pure stretched transition in a large range of the energy E, say, up to 16 MeV, and reaches to the limit of the nonstretched transition, about 0.6, at higher energy, around 19 MeV. Indeed, these features are revealed in the calculated anisotropy for the SDGDR in ^{84}Sr at $I = 48\hbar$, as shown in Fig. 6(b).

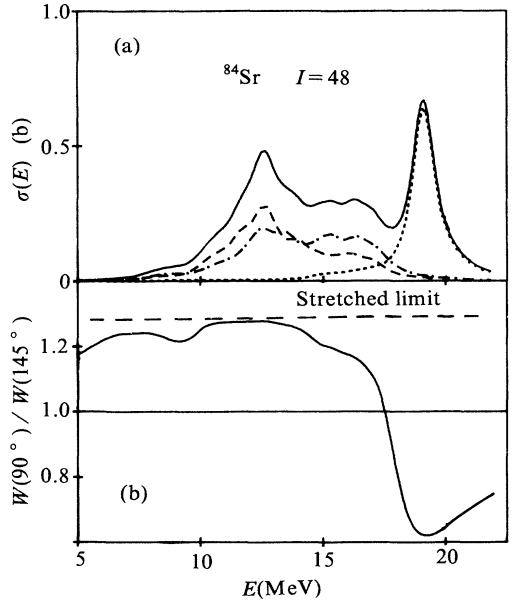

FIG. 6. (a) The total photon absorption cross section with three decomposed resonances for the transitions I to I (dotted), I to $I+1$ (dashed), and I to $I-1$ (dot-dashed), and (b) the anisotropy of the angular distribution for the triaxial SDGDR in ^{84}Sr at $I = 48\hbar$.

IV. SUMMARY

The structure and properties of the SDGDR in $^{146-152}$Dy, $^{132-136}$Nd, and $^{80-84}$Sr even nuclei are studied by means of the linear-response theory with a rotating superdeformed mean field which is obtained by self-consistent calculation. The obtained superdeformed shapes are nearly prolate for all these nuclei except ^{84}Sr which has a triaxial shape instead. The basic features of the SDGDR are that the splitting of the SDGDR is very large. The low-energy components carry about 32%, 26%, and 31% of the EWSR for Dy, Nd, and Sr nuclei, respectively, and are formed from very pure stretched transition γ rays. The calculated FWHM of the low-energy peak is larger than that for the high-energy peak in a SDGDR for all cases of Dy, Nd, and Sr, because an additional fragmentation width is caused by the rotational motion in the low-energy component. The anisotropy of the angular distribution gets the maximum, closing to the limit of the stretched transition, around the centroid energy of the low-energy peak. The isotropic points are much larger than those for the case of normally deformed shape in corresponding nuclei. These common features may serve as the criterion of the observation of SDGDR experimentally. The calculation indicates that a small γ deformation has a considerable effect, much stronger than that for the normally deformed case, on the width and the peak strength of the high-energy component, and thus the self-consistent treatment with respect to γ deformation is necessary to study the fine structure of SDGDR although the SD states are often found to be

nearly prolate shape. The above common features also hold for a superdeformed triaxial shape, but a distinguished new feature is that the large fraction of the total intensity is distributed to bridge the valley between the low- and high-energy peaks, and consequently the anisotropy of angular distribution reaches to the stretched limit in a large range of the energy and to the nonstretched limit around high resonance energy, for example, as seen in the SDGDR for ^{84}Sr.

This work was supported by the National Natural Science Foundation of China.

[1]J. O. Newton, B. Herskind, R. M. Diamond, E. L. Dines, J. E. Draper, K. H. Lindenbeger, C. Schuck, S. Shih, and F. S. Stephens, Phys. Rev. Lett. **46**, 1383 (1981).
[2]J. J. Gaardhoje, C. Ellegaard, B. Herskind, and S. G. Steadman, Phys. Rev. Lett. **53**, 148 (1984).
[3]Kurt A. Snover, Annu. Rev. Nucl. Part. Sci. **36**, 545 (1986).
[4]P. J. Twin *et al.*, Phys. Rev. Lett. **57**, 811 (1886).
[5]E. M. Beck *et al.*, Phys. Lett. B **195**, 531 (1987); E. F. Moore *et al.*, Phys. Rev. Lett. **63**, 360 (1989).
[6]A. M. Bruce, J. J. Gaardhoje, B. Herskind, R. Chapman, J. C. Lisle, F. Khazaie, J. N. Mo, and P. J. Twin, Phys. Lett. B **215**, 237 (1988).
[7]J. L. Egido and P. Ring, Phys. Rev. C **25**, 3239 (1982).
[8]P. Ring, L. M. Robeldo, J. L. Egido, and M. Faber, Nucl. Phys. **A419**, 261 (1984).
[9]M. Gallardo, M. Diebet, T. Dossing, and R. A. Broglia, Nucl. Phys. **A443**, 415 (1985).
[10]K. Sugawara-Tanabe and K. Tanabe, Phys. Lett. B **192**, 268 (1987).
[11]V. M. Sturtinsky, Nucl. Phys. **A95**, 420 (1976).
[12]P. Ring and P. Schuck, *The Nuclear Many Body Problem* (Springer-Verlag, Heidelberg, 1980).
[13]A. Borh and B. R. Mottelson, *Nuclear Structure* (Benjamin, New York, 1975), p. Vol. II.
[14]Y. S. Chen, Chin. J. Nucl. Phys. **11**, 53 (1989).
[15]M. Danos, Nucl. Phys. **5**, 243 (1958).